Supplementary Information

Understanding the local structure of Eu^{3+}- and Y^{3+}- stabilized zirconia: insights from luminescence and X–ray absorption spectroscopic investigations

M. Eibl[1], S. Shaw[2], D. Prieur[1], A. Rossberg[1], M. C. Wilding[3], C. Hennig[1], K. Morris[2], J. Rothe[4], T. Stumpf[1] and N. Huittinen[1]*

[1)]*Helmholtz–Zentrum Dresden–Rossendorf, Institute of Resource Ecology, Bautzner Landstraße 400, 01328 Dresden, Germany*

[2)]*Research Centre for Radwaste Disposal and Williamson Research Centre, School of Earth, Atmospheric and Environmental Science, University of Manchester, Manchester M13 9PL, UK*

[3)]*University of Manchester at Harwell, Diamond Light Source, Harwell Campus, Didcot OX1 0DE*

[4)]*Institute for Nuclear Waste Disposal, Karlsruhe Institute of Technology, Hermann–von–Helmholtz–Platz, 76344 Eggenstein–Leopoldshafen, Germany*

*Corresponding author :

Nina Huittinen
email : n.huittinen@hzdr.de
phone : +49 351 260 2148
fax : +49 351 260 3553

Bulk structural investigations of Eu^{3+}–doped zirconia solid solutions

In Figure S1 SEM–EDX images of a Eu^{3+} doped zirconia sample are shown to visualize the homogeneous distribution of Eu^{3+} within the zirconia matrix.

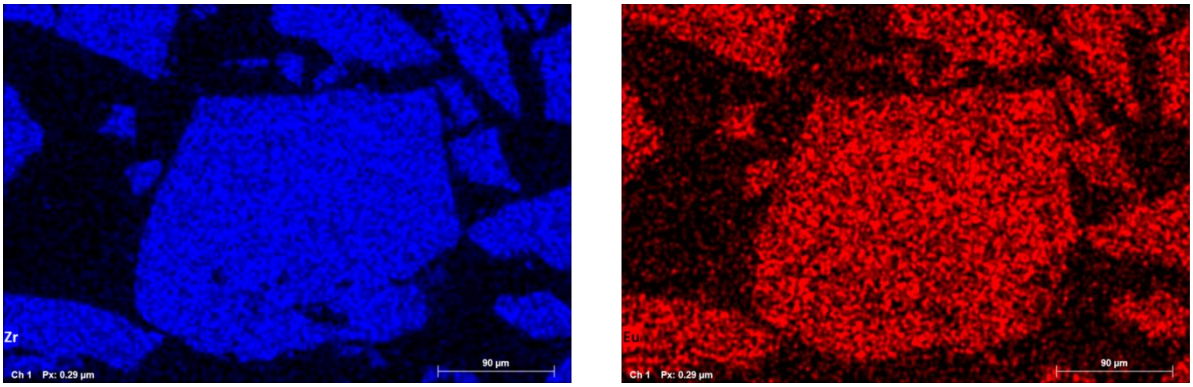

Figure S1: SEM–EDX image of embedded and polished zirconia sample with a Eu^{3+} doping percentage of 24 mol%, showing the distribution of Zr (left, blue) and of Eu (right, red).

In Figure S2 a part of the diffraction patterns of four selected Eu^{3+} doped zirconia samples are presented. The marked reflexes corresponding to planes of the tetragonal or the cubic phases show a strong overlap of diffraction peaks even of high diffraction order, hindering a precise phase quantification.

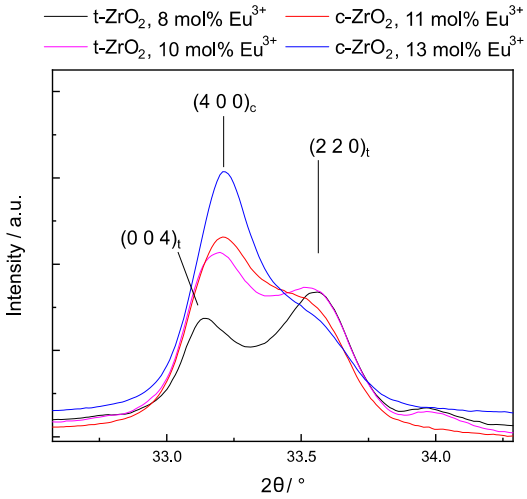

Figure S2: Selected diffraction pattern at different doping fractions, recorded with a wavelength of 0.73804 Å.

In Figure S3 the total diffuse scattering function (S(Q)) of the Eu^{3+} doped zirconia row (16-24 mol%) is presented. No noteworthy change in the diffuse scattering is observed.

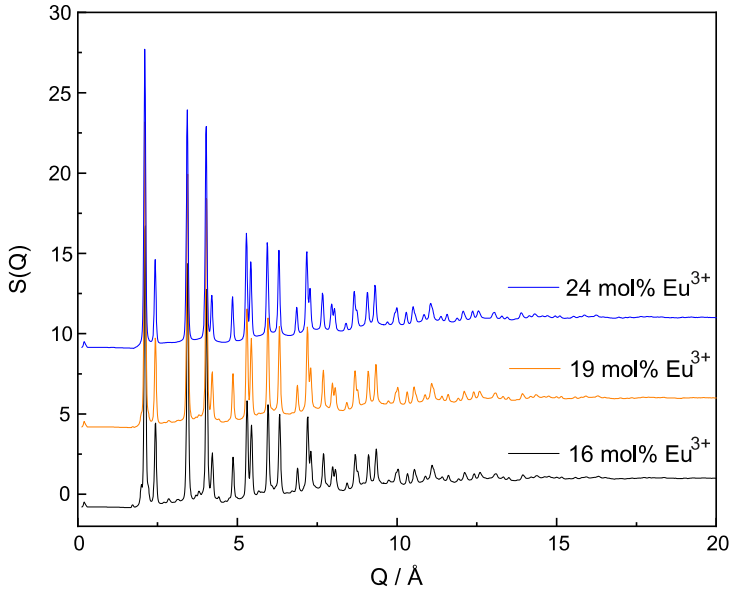

Figure S3: Total scattering functions of zirconia sample row with 16–24 mol% Eu^{3+} doping.

The lattice parameters, obtained by XPDF are compared to the ones resulting from Rietveld refinement of the PXRD data in Table S1.

Table S1: Comparison of lattice parameters obtained by Rietveld refinement of PXRD analysis and XPDF analysis.

Eu^{3+} content / mol%	Lattice parameter of c–ZrO_2 / Å	
	From PXRD	From XPDF
16	5.172 ± 0.005	5.161 ± 0.005
19	5.175 ± 0.005	5.167 ± 0.005
24	5.182 ± 0.005	5.178 ± 0.005

TRLFS studies of Eu^{3+}/Y^{3+} incorporation into ZrO_2

Despite of the high similarities of the phase composition of samples doped with Eu^{3+} or Y^{3+} there are some differences in the luminescence behavior. The excitation spectrum of a sample doped with 16 mol% Y^{3+} is shifted to lower wavelengths by 0.2 nm (Figure S4, top, left). This could be due to a remaining fraction of m-ZrO_2 in the sample, which has a more blue–shifted excitation peak. However, the excitation peak positions of the samples doped with a higher Y–concentration match very well with the purely Eu^{3+} doped samples (s. Figure S4, top right and bottom).

The purely Eu^{3+}-doped samples of high doping (18 and 24 mol%) have a shoulder on the blue–side of the excitation spectra. As it was discussed before that the incorporation into surface layers of zirconia yields an excitation peak at 577.2 nm this shoulder could be related to a higher

fraction of surface layer species. When comparing the crystallite sizes derived from PXRD (s. Table 1 and Figure S8) it can be seen that the only Eu^{3+} doped samples have significantly smaller crystallites and, therefore, a higher surface to bulk site ratio, which speaks for the above stated assignment.

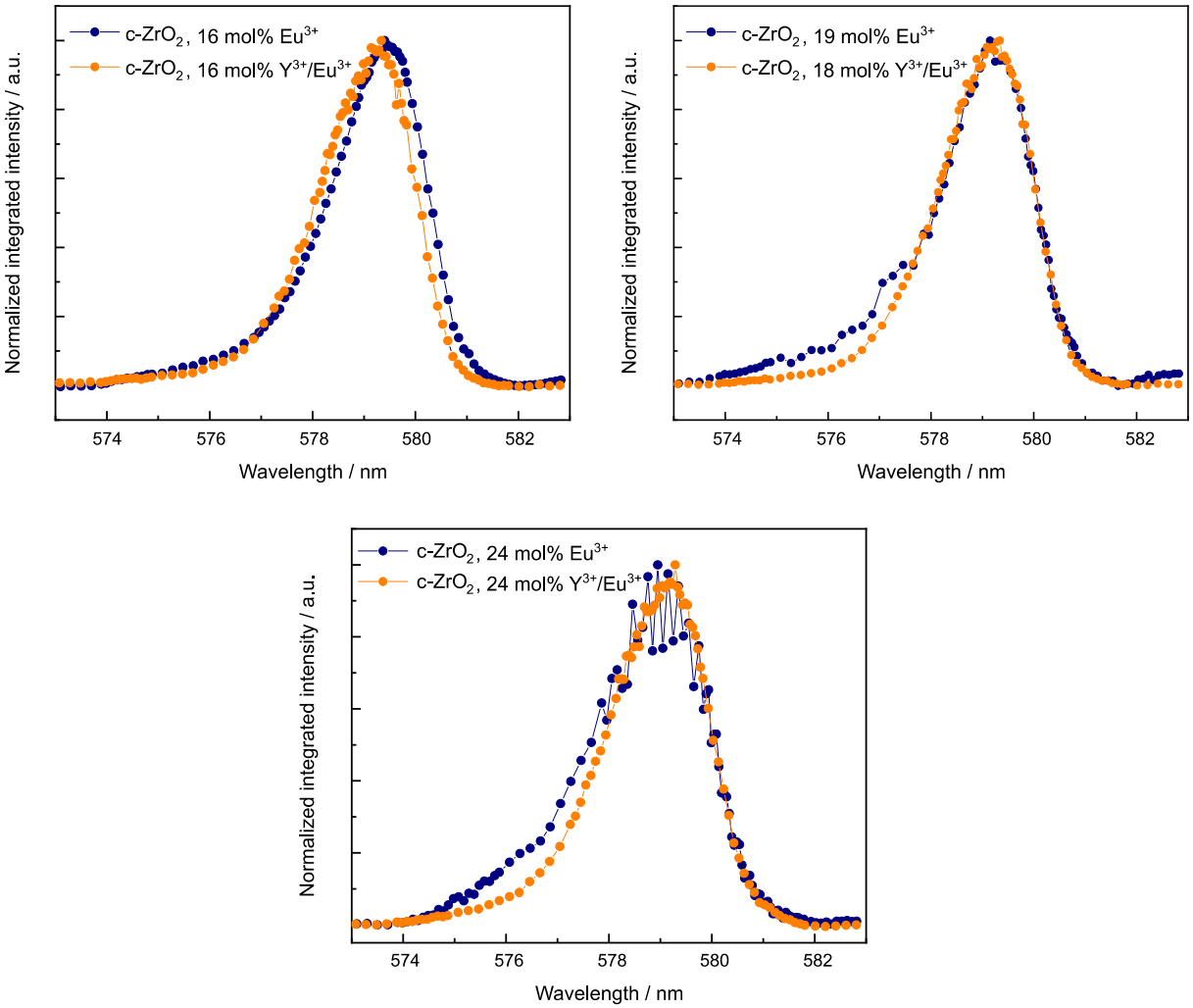

Figure S4: Comparison of the excitation spectra of ZrO_2 doped with Eu^{3+} or Y^{3+}/Eu^{3+} at a doping level of 16 mol% (top, left) 18 mol% (Eu^{3+}) and 19 mol% (Y^{3+}/Eu^{3+}) co-doped (top, right) and 24 mol% (bottom).

In Figure S5 a comparison of the emission patterns of a zirconia sample doped with Eu^{3+}, and of one co–doped with Y^{3+} excited at 579.7 nm are plotted. It can be observed, that the emission peak positions match very well. Therefore, it is assumed that the emission from the purely Eu^{3+} doped samples, which is the same for all the excitation wavelengths used in this manuscript, due to energy transfer processes results from the same Eu^{3+} site as the emission of the Y^{3+} co–doped sample, excited at 579.7 nm.

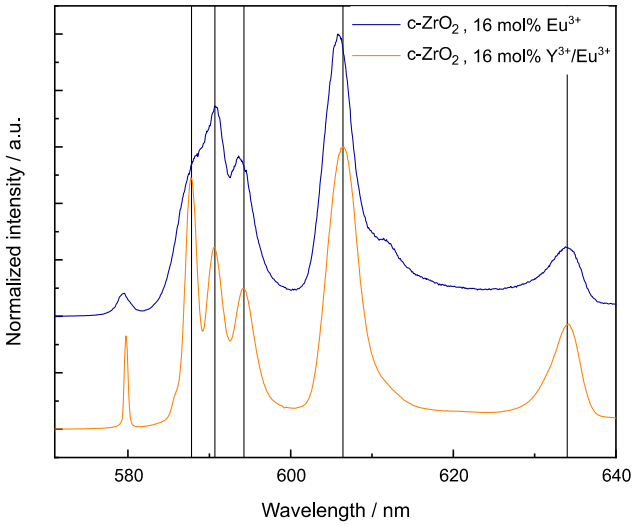

Figure S5: Comparison of the emission spectra of Eu^{3+}-doped zirconia and of Y^{3+}/Eu^{3+} co–doped zirconia with λ_{ex} = 579.7 nm. Black lines are a visualization help only.

In Figure S6, the fluorescence intensity decay of Y^{3+}/Eu^{3+} co–doped zirconia samples are presented for two different excitation wavelengths.

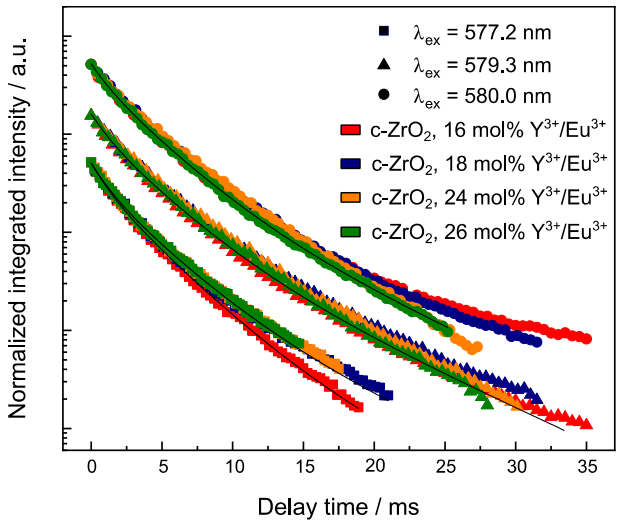

Figure S6: Lifetimes of Y^{3+}/Eu^{3+} co–doped ZrO_2 with doping percentages from 16 mol% to 26 mol% excited at λ_{ex} = 577.2 nm (squares), at λ_{ex} = 579.3 nm (triangles), and at λ_{ex} = 580.0 nm (dots) which are presented with an offset as visualization help. The black lines are examples for the decay curves resulting from fitting the data points.

EXAFS and XPDF studies of the local environment of Eu^{3+}-doped ZrO_2

The normalized absorption spectra of all four Y^{3+}/Eu^{3+} co-doped samples at the Zr (left) and Y K-edge (right) are presented in Figure S7.

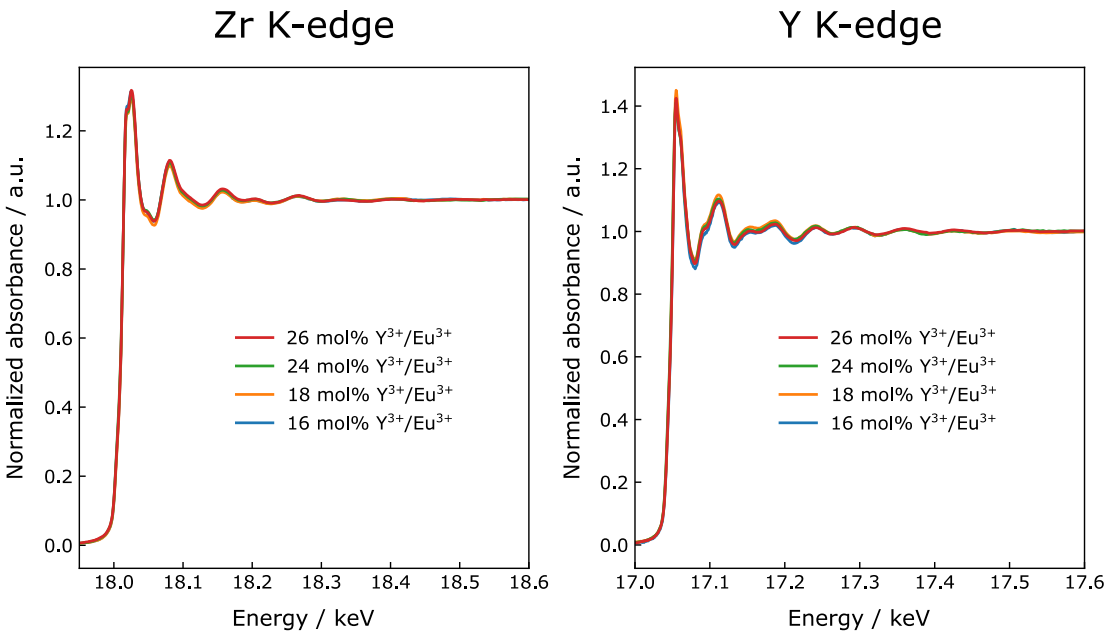

Figure S7: Normalized absorption spectra of Y^{3+}/Eu^{3+} co-doped zirconia in the doping row from 16 – 26 mol% at the Zr K-edge (left) and the Y K-edge (right).

In the following tables, Table S2 and Table S3 – Table S8 the XPDF and EXAFS fitting results, respectively are presented. In the EXAFS–tables, different fitting conditions have been attempted. In Table S3, The CN of the abs–O path is fitted.

Table S2: Atomic distances in Eu^{3+} doped zirconia of 16 – 24 mol% derived by XPDF.

Eu^{3+} doping / mol%	Atomic distances / Å			
	Zr–O	Eu–O	Zr–M	Zr–O/Eu–O
16	2.11 ± 0.02	2.39 ± 0.02	3.61 ± 0.02	4.35 ± 0.02
18	2.12 ± 0.02	2.38 ± 0.02	3.61 ± 0.02?	4.32 ± 0.02
24	2.11 ± 0.02	2.38 ± 0.02	3.62 ± 0.02	4.30 ± 0.02

In Table S3 the resulting CNs, where the abs–O path was fitted are presented.

Table S3: Structural parameters derived from the k^3–weighted EXAFS spectra for the Zr and the Y K–edge. Fixed CN are marked with an asterisk (*). Abs–O CN is fitted here. Fitting range is 2 – 10.5 $Å^{-1}$, R: radial distance, error ± 0.01 Å, CN: coordination number, error ± 20%, σ^2: Debye–Waller factor, error ± 0.001 Å, amplitude reduction factor (S_0^2) = 1.0, number of independent points = 16. The average R-values of the Zr K-edge fits and the Y K-edge fits are 7.3 ± 1.2 and 6.2 ± 0.7, respectively.

Y^{3+} content / mol%	Path	Zr K–edge R / Å	CN	σ^2 / $Å^2$	Y K–edge R / Å	CN	σ^2 / $Å^2$
16	abs–O	2.14	6.13	0.009	2.32	7.9	0.010
	abs–M	3.54	12*	0.014	3.61	12*	0.009
	abs–O–abs	3.90	48*	0.020	4.20	48*	0.008
	abs–O	4.52	24*	0.101	4.50	24*	0.033
18	abs–O	2.15	7.70	0.012	2.31	7.0	0.009
	abs–M	3.56	12*	0.014	3.61	12*	0.010
	abs–O–abs	3.93	48*	0.025	4.20	48*	0.005
	abs–O	4.36	24*	0.044	4.48	24*	0.036
24	abs–O	2.16	7.03	0.011	2.32	8.2	0.013
	abs–M	3.56	12*	0.013	3.61	12*	0.010
	abs–O–M	3.83	48*	0.028	4.20	48*	0.006
	abs–O	4.41	24*	0.055	4.49	24*	0.030
26	abs–O	2.14	7.44	0.011	2.31	7.2	0.010
	abs–M	3.55	12*	0.013	3.61	12*	0.010
	abs–O–M	3.93	48*	0.028	4.10	48*	0.012
	abs–O	4.35	24*	0.050	4.47	24*	0.043

The fitting results, where the CN of the abs–M path is fitted, are presented in Table S4.

Table S4: Structural parameters derived from the k^3–weighted EXAFS spectra for the Zr and the Y K–edge. Fixed CN are marked with an asterisk (*). Abs–M CN is fitted here. Fitting range is 2 – 10.5 $Å^{-1}$, R: radial distance, error ± 0.01 Å, CN: coordination number, error ± 20%, σ^2: Debye–Waller factor, error ± 0.001 Å, amplitude reduction factor (S_0^2) = 1.0, number of independent points = 16. The average R-values of the Zr K-edge fits and the Y K-edge fits are 8.13 ± 1.5 and 6.3 ± 0.4, respectively.

Y^{3+} content / mol%	Path	Zr K–edge			Y K–edge		
		R / Å	CN	σ^2 / $Å^2$	R / Å	CN	σ^2 / $Å^2$
16	abs–O	2.13	8*	0.012	2.32	8*	0.010
	abs–M	3.56	13.27	0.014	3.62	18.9	0.011
	abs–O–M	3.93	48*	0.006	4.01	48*	0.006
	abs–O	4.37	24*	0.086	4.59	24*	0.064
18	abs–O	2.15	8*	0.013	2.31	8*	0.011
	abs–M	3.56	9.97	0.013	3.62	18.36	0.012
	abs–O–M	3.61	48*	0.033	4.04	48*	0.009
	abs–O	4.49	24*	0.068	4.60	24*	0.060
24	abs–O	2.15	8*	0.013	2.32	8*	0.012
	abs–M	3.56	9.30	0.012	3.61	11.99	0.010
	abs–O–M	3.66	48*	0.033	4.17	48*	0.006
	abs–O	4.47	24*	0.064	4.49	24*	0.030
26	abs–O	2.14	8*	0.011	2.31	8*	0.012
	abs–M	3.55	10.97	0.013	3.61	18.52	0.012
	abs–O–M	3.58	48*	0.038	4.01	48*	0.004
	abs–O	4.52	24*	0.073	4.60	24*	0.083

In Table S5 the CN of the abs–O and the abs–M path is fitted.

Table S5: Structural parameters derived from the k^3–weighted EXAFS spectra for the Zr and the Y K–edge. Fixed CN are marked with an asterisk (*). Abs–O and Abs–M CN is fitted here. Fitting range is 2 – 10.5 $Å^{-1}$, R: radial distance, error ± 0.01 Å, CN: coordination number, error ± 20%, σ^2: Debye–Waller factor, error ± 0.001 Å, amplitude reduction factor (S_0^2) = 1.0, number of independent points = 16. The average R-values of the Zr K-edge fits and the Y K-edge fits are 6.9 ± 1.1 and 6.2 ± 0.5, respectively.

Y^{3+} content / mol%		Zr K–edge			Y K–edge		
	Path	R / Å	CN	σ^2 / $Å^2$	R / Å	CN	σ^2 / $Å^2$
16	abs–O	2.14	5.75	0.008	2.32	8.0	0.010
	abs–M	3.57	13.85	0.013	3.62	19.26	0.011
	abs–O–M	3.94	48*	0.002	4.01	48*	0.006
	abs–O	4.57	24*	0.104	4.6**	24*	0.062
18	abs–O	2.15	7.60	0.012	2.31	7.06	0.009
	abs–M	3.56	9.88	0.013	3.62	17.83	0.012
	abs–O–M	3.63	48*	0.032	4.05	48*	0.008
	abs–O	4.49	24*	0.070	4.6**	24*	0.06**
24	abs–O	2.16	7.41	0.011	2.32	8.16	0.013
	abs–M	3.55	10.91	0.013	3.61	12.06	0.010
	abs–O–M	3.68	48*	0.028	4.17	48*	0.064
	abs–O	4.48	24*	0.067	4.49	24*	0.030
26	abs–O	2.14	7.41	0.011	2.31	6.93	0.010
	abs–M	3.55	10.91	0.013	3.62	16.97	0.011
	abs–O–M	3.61	48*	0.039	4.01	48*	0.002
	abs–O	4.52	24*	0.078	4.94	24*	0.026

In Table S6 the fitting results are shown, where the abs–O–abs–O scatter path is additionally included into the fit.

Table S6: Structural parameters derived from the k^3–weighted EXAFS spectra for the Zr and the Y K–edge. Fixed CN are marked with an asterisk (*). Abs–O–abs–O shell is fitted additionally, here. Fitting range is 2 – 10.5 $Å^{-1}$, R: radial distance, error ± 0.01 Å, CN: coordination number, error ± 20%, σ^2: Debye–Waller factor, error ± 0.001 Å, amplitude reduction factor (S_0^2) = 1.0, number of independent points = 16. The average R-values of the Zr K-edge fits and the Y K-edge fits are 7.8 ± 1.1 and 6.3 ± 0.6, respectively.

Y^{3+} content / mol%		Zr K–edge			Y K–edge		
	Path	R / Å	CN	σ^2 / $Å^2$	R / Å	CN	σ^2 / $Å^2$
16	abs–O	2.14	8*	0.012	2.32	8*	0.010
	abs–M	3.54	12*	0.014	3.61	12*	0.009
	abs–O–M	3.89	48*	0.018	4.17	48*	0.009
	abs–O	4.59	24*	0.047	4.38	24*	0.045
	abs–O–abs–O	4.28	8*	0.024	4.64	8*	0.021
18	abs–O	2.14	8*	0.012	2.31	8*	0.011
	abs–M	3.55	12*	0.013	3.61	12*	0.010
	abs–O–M	3.87	48*	0.020	4.14	48*	0.005
	abs–O	4.60	24*	0.045	4.32	24*	0.046
	abs–O–abs–O	4.29	8*	0.025	4.63	8*	0.021
24	abs–O	2.15	8*	0.011	2.31	8*	0.012
	abs–M	3.55	12*	0.013	3.61	12*	0.009
	abs–O–M	3.84	48*	0.017	4.17	48*	0.008
	abs–O	4.62	24*	0.042	4.38	24*	0.050
	abs–O–abs–O	4.30	8*	0.026	4.63	8*	0.025
26	abs–O	2.14	8*	0.011	2.31	8*	0.012
	abs–M	3.55	12*	0.013	3.60	12*	0.010
	abs–O–M	3.87	48*	0.018	4.14	48*	0.012
	abs–O	4.60	24*	0.044	4.30	24*	0.045
	abs–O–abs–O	4.28	8*	0.023	4.62	8*	0.023

In Table S7 the second abs–O shell isn't included in the fit.

Table S7: Structural parameters derived from the k^3–weighted EXAFS spectra for the Zr and the Y K–edge. Fixed CN are marked with an asterisk (*). The second abs–O shell wasn't fitted here. Fitting range is 2 – 10.5 $Å^{-1}$, R: radial distance, error ± 0.01 Å, CN: coordination number, error ± 20%, σ^2: Debye–Waller factor, error ± 0.001 Å, amplitude reduction factor (S_0^2) = 1.0, number of independent points = 16. The average R-values of the Zr K-edge fits and the Y K-edge fits are 8.2 ± 2.1 and 7.0 ± 1.0, respectively.

Y^{3+} content / mol%		Zr K–edge			Y K–edge		
	Path	R / Å	CN	σ^2 / $Å^2$	R / Å	CN	σ^2 / $Å^2$
16	abs–O	2.14	8*	0.012	2.31	8*	0.010
	abs–M	3.54	12*	0.014	3.61	12*	0.009
	abs–O–M	3.92	48*	0.017	4.10	48*	0.012
18	abs–O	2.15	8*	0.013	2.31	8*	0.011
	abs–M	3.56	12*	0.014	3.61	12*	0.010
	abs–O–M	3.69	48*	0.062	4.12	48*	0.005
24	abs–O	2.15	8*	0.013	2.31	8*	0.012
	abs–M	3.55	12*	0.014	3.61	12*	0.009
	abs–O–M	3.75	48*	0.029	4.10	48*	0.001
26	abs–O	2.14	8*	0.011	2.31	8*	0.012
	abs–M	3.55	12*	0.014	3.60	12*	0.010
	abs–O–M	3.67	48*	0.045	4.10	48*	0.013

In Table S8, the fitting results using only the abs–O and the abs–M path are presented.

Table S8: Structural parameters derived from the k^3–weighted EXAFS spectra for the Zr and the Y K–edge. Fixed CN are marked with an asterisk (*). Only first abs–O shell and abs–M shell is fitted here. Fitting range is 2 – 10.5 $Å^{-1}$, R: radial distance, error ± 0.01 Å, CN: coordination number, error ± 20%, σ^2: Debye–Waller factor, error ± 0.001 Å, amplitude reduction factor (S_0^2) = 1.0, number of independent points = 16. The average R-values of the Zr K-edge fits and the Y K-edge fits are 9.2 ± 2.0 and 7.5 ± 1.7, respectively.

Y^{3+} content / mol%		Zr K–edge			Y K–edge		
	Path	R / Å	CN	σ^2 / $Å^2$	R / Å	CN	σ^2 / $Å^2$
16	abs–O	2.13	8*	0.012	2.32	8*	0.010
	abs–M	3.54	12*	0.015	3.61	12*	0.008
18	abs–O	2.14	8*	0.013	2.32	8*	0.011
	abs–M	3.55	12*	0.014	3.61	12*	0.009
24	abs–O	2.15	8*	0.013	2.31	8*	0.013
	abs–M	3.55	12*	0.014	3.61	12*	0.009
26	abs–O	2.14	8*	0.011	2.31	8*	0.012
	abs–M	3.55	12*	0.014	3.61	12*	0.009

Gaussian fitting of site–selective TRLFS excitation spectra

The results of the Gaussian fitting of all the TRLFS excitation spectra are presented in Figure S8.

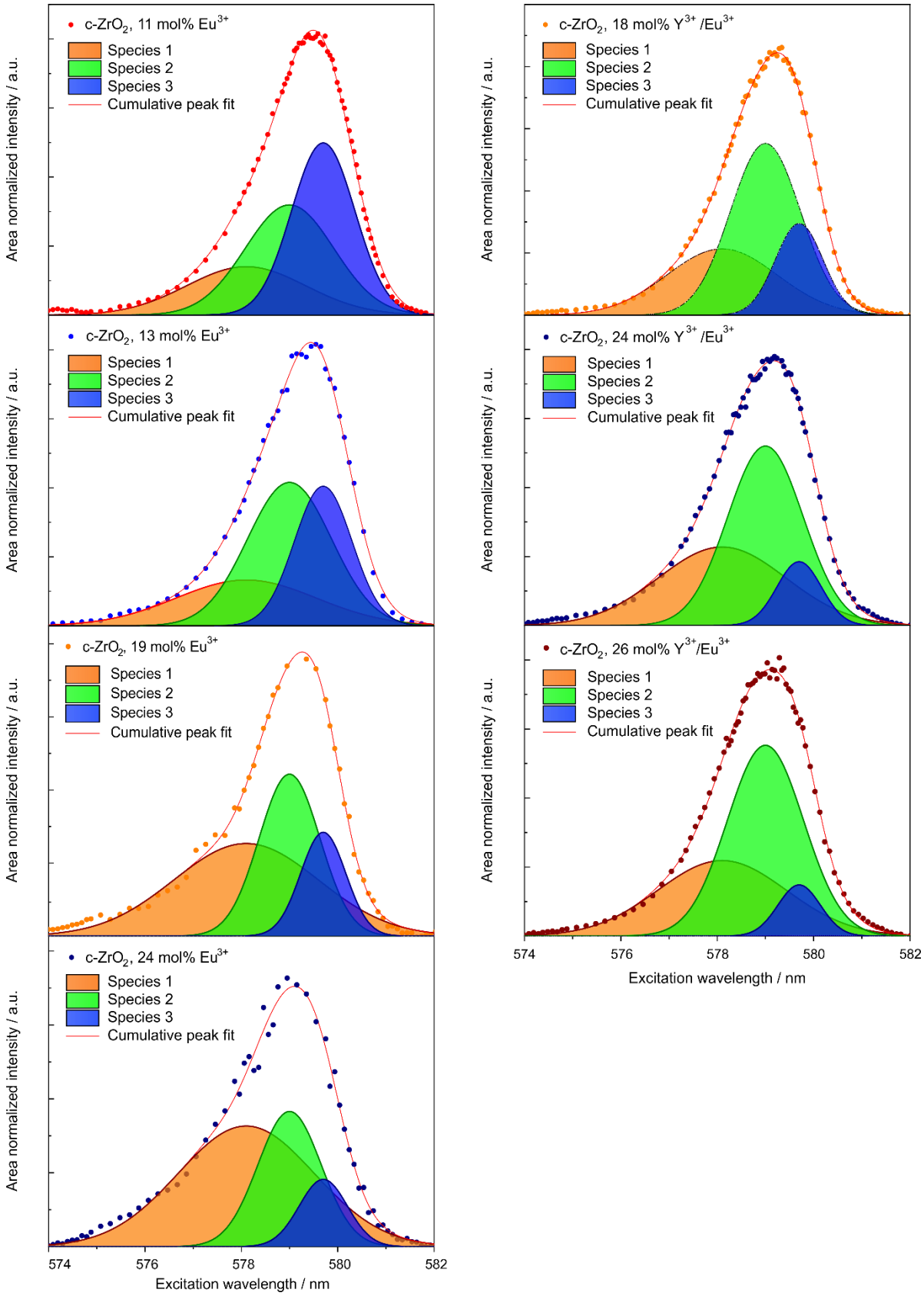

Figure S8: Gaussian fits of excitation spectra collected for Eu^{3+} concentrations of 11, 13, 19 and 24 mol% (from top to bottom, left) and Y^{3+}/Eu^{3+} co–doped c–ZrO_2 with doping concentrations of 18, 24 and 26 mol% (from top to bottom, right).

Effect of crystallite size on the distribution of species 1

In Figure S9, a comparison of the phase percentage of species 1, derived from fitting of the TRLFS excitation spectra, with the crystallite size, obtained from diffraction peak broadening is presented for samples doped with Eu^{3+} only (left) and for Y^{3+}/Eu^{3+} co–doped zirconia (right).

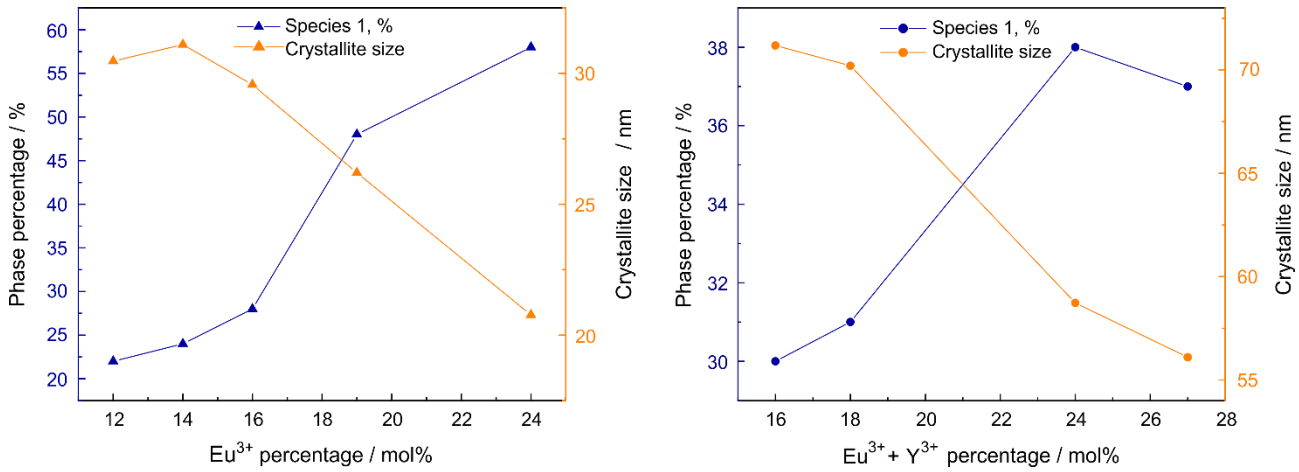

Figure S9: Comparison of the phase percentage of species 1 in the site–selective TRLFS excitation spectra, determined by Gaussian peak fitting with the crystallite size derived from PXRD for Eu^{3+}-doped (left) and Y^{3+}/Eu^{3+} co–doped zirconia samples (right).

The number of oxygen vacancies in dependence of the trivalent doping fraction is presented in Figure S10 along with the amount of Zr and Eu atoms with an oxygen vacancy in the first coordination sphere when assuming a statistical distribution with no preferential oxygen vacancy location. Since the oxygen atoms in ZrO_2 are coordinated to four cations, every oxygen vacancy will influence four Zr and/or dopant ions in the crystal lattice. It further implies that only up to 50 mol% trivalent dopant can be theoretically hosted without more than one oxygen vacancy in each cation NN coordination. Therefore, values at higher doping levels are larger than 100, indicating that the presence of two oxygen vacancies in some cation NN coordination spheres are necessary.

The number of Eu^{3+} cations per 100 overall cations (Eu+Zr(+Y)) with one oxygen vacancy (O_{vac}), assuming statistical follows the equation:

$$N\left(Eu_{O_{vac}}\right) = 200 * x(Eu)^2 \qquad (Eq.S1)$$

The number of Zr^{4+} cations per 100 overall cations (Eu + Zr (+ Y)) with one O_{vac}, assuming statistical distribution follows the equation:

$$N\left(Eu_{O_{vac}}\right) = 200 * (x(Eu) - x(Eu)^2) \qquad (Eq.S2)$$

The number of O_{vac} follows equation S3.

$$N(O_{vac}) = 50 * x(Eu) \qquad (Eq.S3)$$

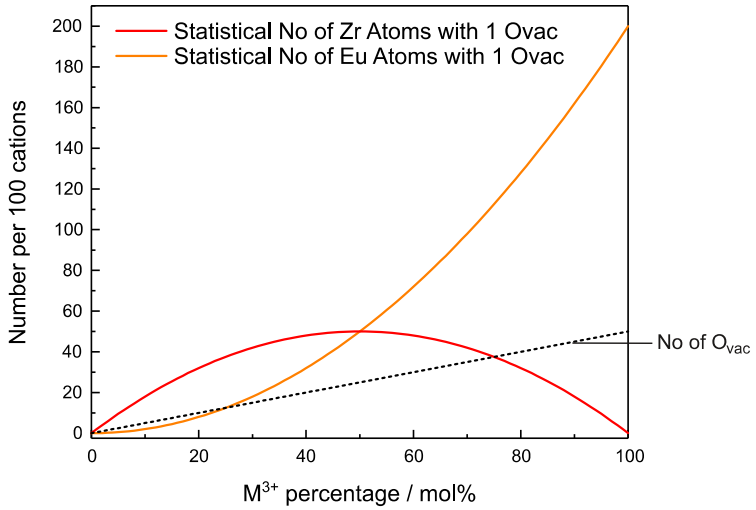

Figure S10: Number of oxygen vacancies created in the ZrO_2 lattice (black, dotted line) and number of cations with an oxygen vacancy in the first coordination sphere of Eu (orange line) or Zr (red line), assuming a non-preferential, statistical distribution. Numbers larger than 100 result from the necessity of two oxygen vacancies in the coordination sphere of one cation.

Fluorescence lifetimes of Y^{3+}/Eu^{3+} co-doped zirconia

In order to assign the measured luminescence lifetimes to individual Eu^{3+} environments (species 1, 2, and 3) in the solid structure, delayed excitation spectra were measured 8 ms after the laser pulse. This delayed excitation spectrum (black symbols) is compared in Figure S11 to the excitation spectrum measured after 1 µs delay.

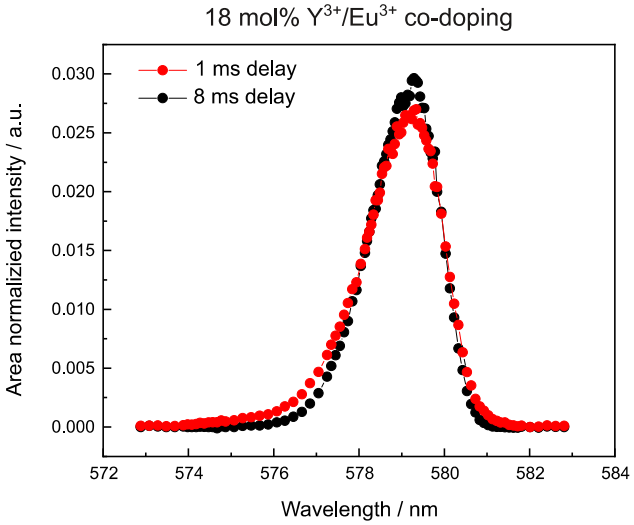

Figure S11: Comparison of the excitation spectrum of a Y^{3+}/Eu^{3+} co-doped zirconia sample (18 mol% doping) measured with a delay of 1 µs and measured with 8 ms delay after the laser pulse.